

Effect of Sandblasting on Tensile Properties, Hardness and Fracture Resistance of a Line Pipe Steel Used in Algeria for Oil Transport

O. Bouledroua · M. Hadj Meliani · Z. Azari · A. Sorour ·
N. Merah · G. Pluinage

Submitted: 9 March 2017 / in revised form: 11 May 2017 / Published online: 4 August 2017
© ASM International 2017

Abstract Transport of oil and gas through pipelines in the harsh conditions of the Algerian desert, results in erosion of the pipeline materials. Erosion is a mechanical process that causes a loss of wall thickness, damage and residual stresses on the surface of a pipe due to shocks between sand particles and structure surface. Damage manifests by spalling craters of different shapes and depths. The evaluation of tensile properties and hardness after sandblasting for different durations has been performed on API 5L X70 pipeline steel. Particular attention has been paid to fracture resistance after sandblasting to provide the necessary data for defect assessment, specially the effect of sandblasting on the Material Failure Master Curve (MFMC). The results demonstrated that the sandblasting has slightly increased the yield stress, the ultimate strength and the fracture toughness and, at the same time, had an adverse effect on elongation, young's modulus, hardness and thickness of the tested pipeline.

Keywords API 5L X70 steel · Erosion · Sandblasting · Tensile strength · Hardness

Introduction

High strength steels, such as API 5L X70 and beyond, possess highly refined grains and cleanliness. Pipelines made of these types of steels are often subjected to severe erosion due to transportation of petroleum products which is accompanied by erodent particles [1, 2]. Material loss due to sand erosion can cause severe damage to oil and gas pipeline and lead to ruptures if left undetected and unmitigated.

Sandblasting is one of the most effective methods employed to modify internal and/or external metal surfaces in order to improve its properties for repair applications, such as patching. Two techniques for internal and external surface sandblasting are performed, either manually or automatically. Manual sandblasting is the dominant practice in Algeria.

A number of researchers have studied the different effects of sandblasting and erosion [3–7] on the integrity of pipes. Hattori and Nakao [3] studied the cavitation erosion mechanisms through the observation of removed particles for AISI 1015 carbon steel and heat-treated S55C light carbon steel. They divided the phenomenon of erosion into four consecutive stages: the initial stage characterized by high volume/mass loss rate, the incubation stage characterized by cracks caused by the accumulation of plastic deformation, the acceleration stage and the maximum rate stage where the original surface is completely removed. They concluded that the erosion should be evaluated in terms of parameters that include not only the static properties but also the kind of

O. Bouledroua · M. Hadj Meliani (✉)
LPTPM, Hassiba BenBouali University of Chlef, 02000 Chlef,
Algeria
e-mail: m.hadjmeliani@univhb-chlef.dz

M. Hadj Meliani · Z. Azari · G. Pluinage
LaBPS-ENIMI, Paul Verlaine University of Metz, Ile de Saulcy,
57045 Metz, France

A. Sorour
Center of Research Excellence in Corrosion (CoRE-C), King
Fahd University of Petroleum and Minerals, P.O. Box 5040,
Dhahran 31261, Saudi Arabia

N. Merah
Mechanical Department, King Fahd University of Petroleum and
Minerals, P.O. Box 5040, Dhahran 31261, Saudi Arabia

fracture mechanism. Suyitno et al. [4] investigated the effects of cold working and sandblasting on the microhardness distribution, tensile strength and corrosion rate of AISI 316L stainless steel. They found that sandblasting treatment increases the microhardness only at the surface and enhances the surface roughness. Alhussein et al. [5, 6] studied the influence of sandblasting and hydrogen on tensile and fatigue properties of API 5L X52 pipeline steel. They have shown that sandblasting has little effect on the yield stress and ultimate strength, while failure strain and lifetime are improved. Okonkwo et al. [7] investigated the erosive wear performance of API 5L X42 pipeline steel, using a sandblaster erosion machine at a constant angle. Their results showed that sandblasting at high velocities and longer durations caused plowing of the surface. Lopez [8] studied the effect of abrasive velocity and concluded that surface damage increases with increasing impact velocity of the particles. Islam et al. [9] recently studied the erosion–corrosion behavior of API 5L X70 steel by carrying out cyclic erosion and corrosion tests on the steel surface and, hence, determined that the erosion rate of the steel increases with increasing particle velocity. The higher the impact velocity, the higher the kinetic energy, and the deeper the abrasive particle penetrates into the matrix causing accelerated material removal. Majid et al. [10] found that multiple failures of API 5L X42 natural gas pipelines were caused by a water jet from a failed nearby water pipe entraining the surrounding sand particles, which caused erosion. Other studies have shown that erosion rate increases with increasing impact angle up to 90° for brittle materials, while maximum erosion rate occurs between 15° and 45° in ductile materials [11]. Chintapalli et al. [12] reported that sandblasting with particle sizes equal or less than 110 µm and pressures less than 4 bars increases the biaxial strength and the reliability by inducing compressive residual stresses, which counteract the damage induced by sandblasting.

In this paper, the results from sandblasting test are described to study its effects on mechanical properties of API 5L X70 pipeline steel. It includes sandblasting effects on tensile properties, hardness, impact strength and fracture toughness. The influence of sandblasting is coupled with constraint (T-stress is used as constraint parameter) to show the effects on the Material Failure Master Curve (MFMC).

Experimental Procedure

All the specimens used in this study were prepared from 48-inch diameter API 5L X70 steel pipes manufactured and coated by AlfaPipe™ tuberie of Annaba, Algeria, and sandblasting was performed in Ferrovia-Annaba™. These pipes, with an outer diameter of 1219.2 mm and a thickness of 13.10 mm, are used for the transportation of hydrocarbons (crude oil, natural gas, LPG and condensate) [13].

Chemical Composition, Microstructure and Mechanical Properties

The chemical composition of the studied API 5L X70 pipeline steel is illustrated in Table 1. The microstructure of a transverse cross section of the API 5L X70 pipeline steel was analyzed by an optical microscope after mechanical polishing and chemical etching with Nital. Figure 1 shows that the microstructure is composed of fine grains of ferrite base and pearlite colored in white and black, respectively.

Sandblasting Setup

The sandblasting of all specimens is performed using the machine presented in Fig. 2a. The abrasive particle velocity used in this study was 31.83 m/s, with nozzle diameter of 10 mm, and standard pressure 7 bar with an air flow of 600 l/min. The procedures of the sandblasting test; distance between

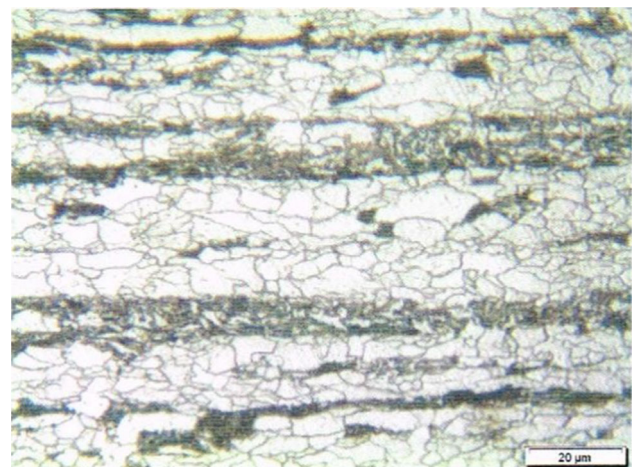


Fig. 1 Microstructure in transverse section of investigated API 5L X70 pipeline steel (Nital etch)

Table 1 Chemical composition of the investigated API 5L X70 pipeline steel

| % | C | Mn | Si | Cr | Ni | Mo | S | Cu | Ti | Nb | Al | P |
|---|-------|------|------|-------|------|-------|-------|-------|-------|-------|-------|-------|
| | 0.125 | 1.68 | 0.27 | 0.051 | 0.04 | 0.021 | 0.005 | 0.045 | 0.003 | 0.033 | 0.038 | 0.012 |

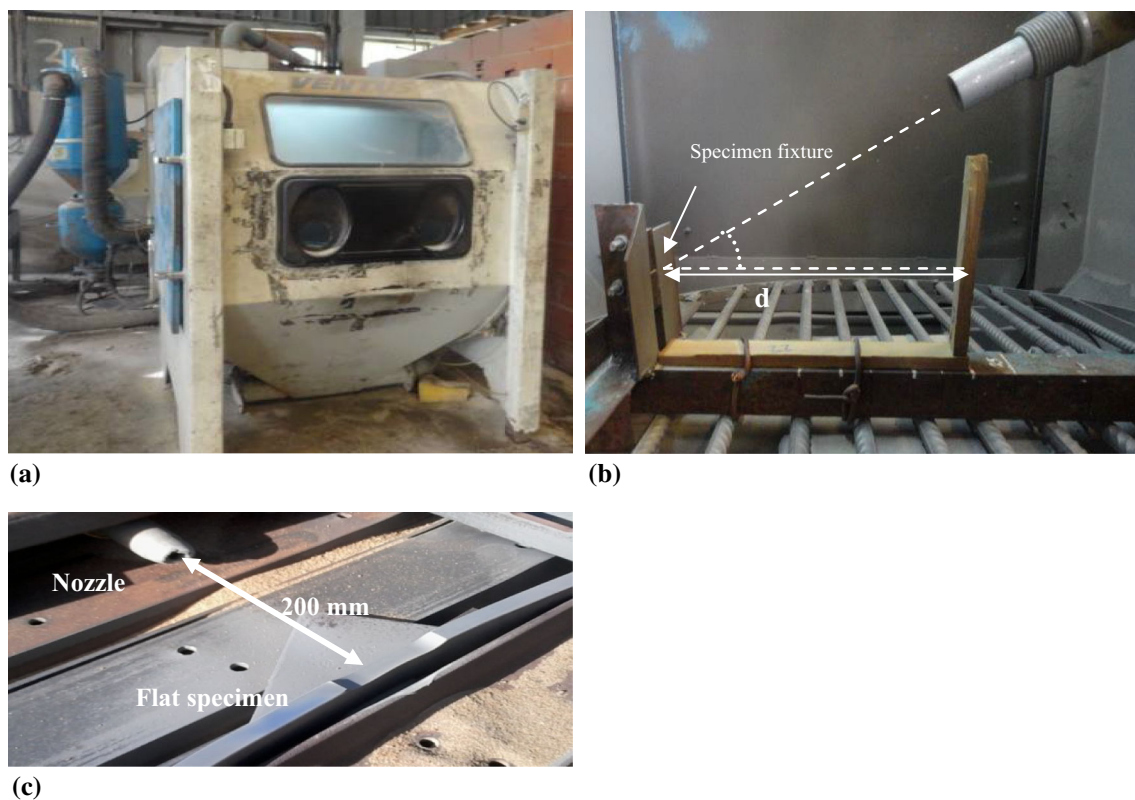


Fig. 2 (a) Sandblasting machine, (b) the angle of sandblasting with the fixture of the V-notch impact specimen and (c) the tensile specimen holder assembly

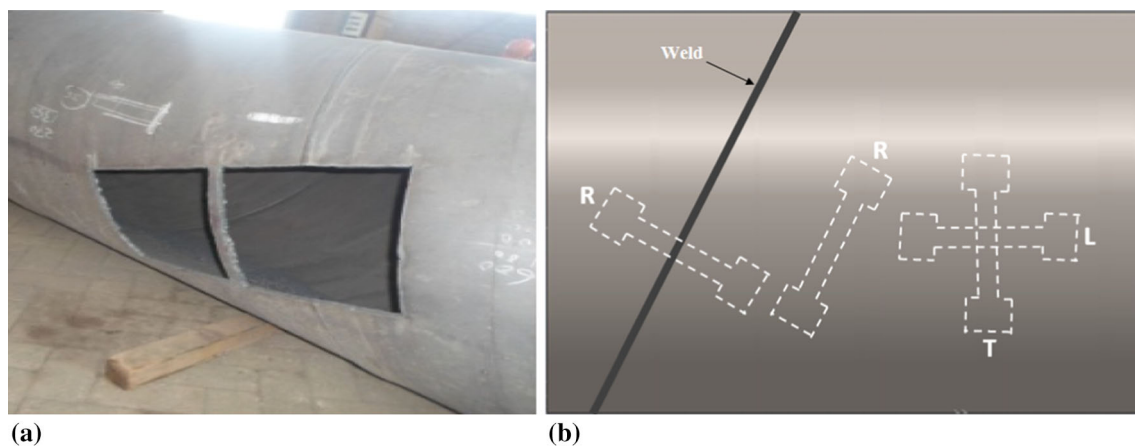


Fig. 3 Square or rectangular cross-joint tensile test specimen (a) and the tensile specimen direction used with R: rolling, L: longitudinal and T: transversal (b)

the nozzle and the specimen (d), the angle orientation of the nozzle (θ) and assembly for the specimen holders are illustrated in Fig. 2b and c.

Tensile, Charpy and Hardness Testing

Following ISO 15614 [14] and ASME 9 [15], tensile specimens were cut from base material and weld area as

shown in Fig. 3. The excess weld metal in the cap of the weld was machined off. The geometry, orientations (R: rolling, T: transversal and L: longitudinal) and dimensions of the tensile specimens are illustrated in Figs. 3 and 4.

The impact toughness of as-received and sandblasted material was measured using Charpy V-notch impact specimens that were prepared according to EN 10045-1 standards [16]. Different ($10 \times 10 \times 55$ mm) Charpy specimens with

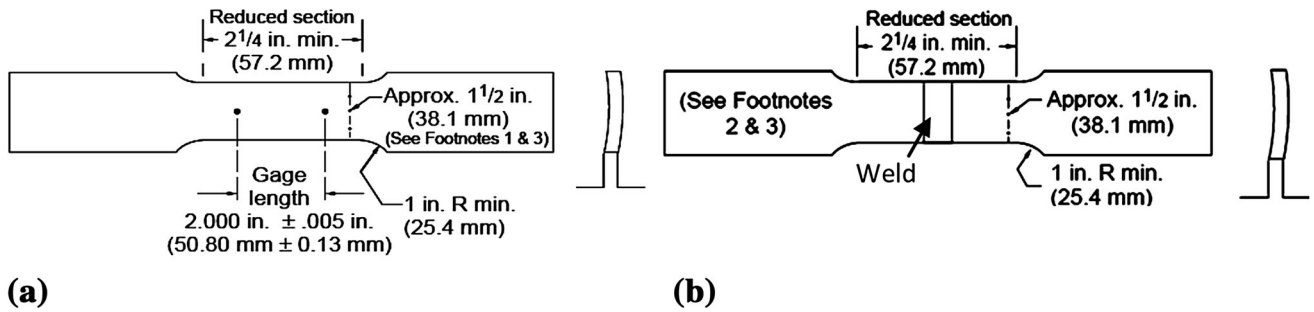


Fig. 4 Geometry and dimensions of strip specimen obtained from (a) base metal (BM) and (b) welded metal (WM)

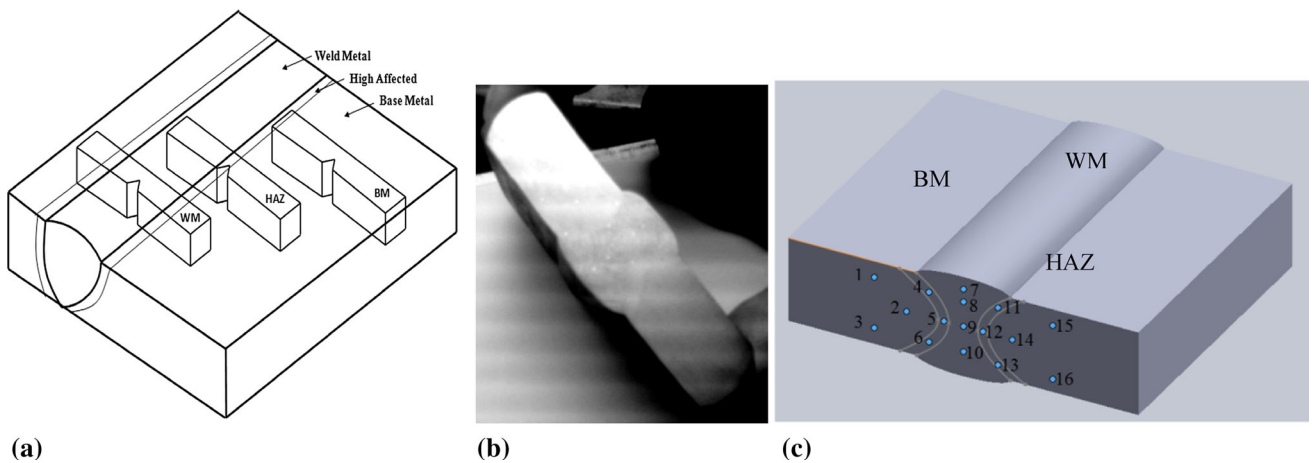


Fig. 5 (a) Schematic representation of Charpy test specimen, (b) specimen for hardness testing and (c) positions at which hardness was measured

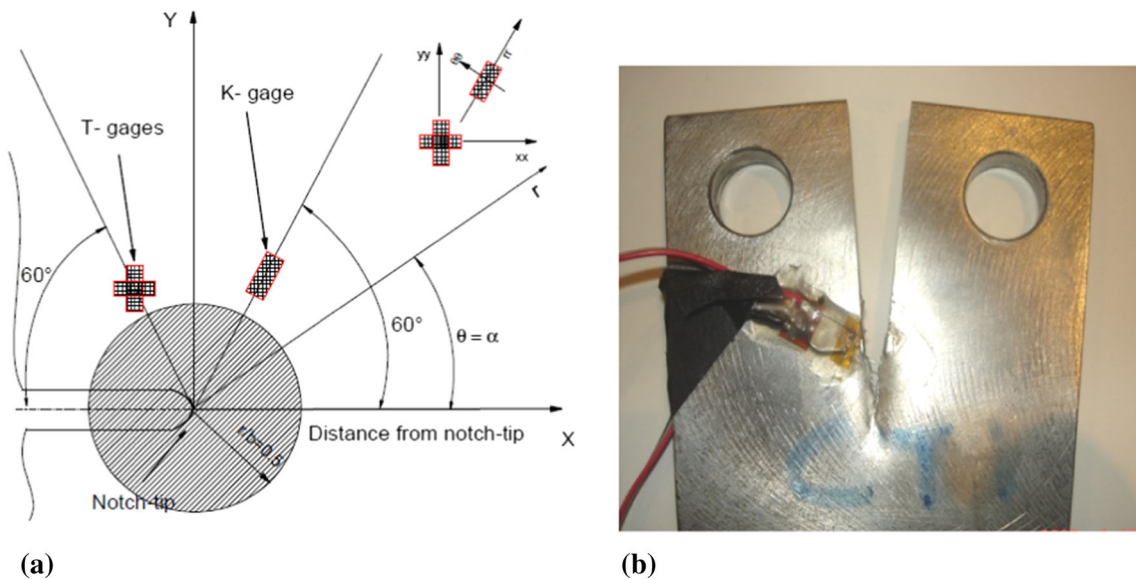


Fig. 6 (a) Schematic representation of position of the gages near the notch tip and (b) CT specimen with the strain gages, after loading

a 2-mm V-notch, positioned in base metal (BM), heat-affected zone (HAZ) and welding metal (WM), were machined as shown in Fig. 5a. Charpy V-notch impact tests were conducted at ambient temperature using a Zwick Z HV10 universal testing machine with a load capacity of 10 kg.

The specimens for hardness measurements were prepared according to ASTM E92-82 standard [17]. Figure 5b shows the specimen used for hardness testing, and Fig. 5c illustrates the positions at which hardness was measured.

Experimental Method to Determine T_{ef} and K_{ef} and Specimens

The Master Failure Material Curve (MFMC) is built in order to create a material characteristic taking into account specimen geometries, ligament sizes, type of steel, loading conditions and environment situations. To get different assessment points (K_{ρ}, T_{ef}), four geometries, namely CT (width of $W = 63.80$ mm, height of 61 mm), DCB (height of $W = 45.70$ mm), SENT (width of $W = 58.40$ mm) and RT (width of 40 mm), were extracted from a steel pipe of external diameter 1219.2 mm. Thickness of all specimens was equal to 5.8 mm. The specimens had a notch with a notch angle $\phi = 0$ and a notch radius $\rho = 0.25$ mm. For the K_{ρ} parameter and the T_{ef} -stress determination ahead of the notch tip, strain gauges were glued in directions shown

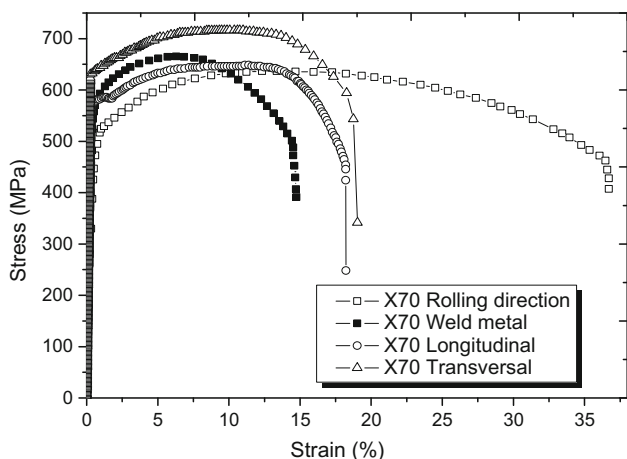


Fig. 7 Typical stress–strain curves of tensile specimens extracted from API 5L X70 pipeline steel

in Fig. 6a at a point located at $r = 3$ mm from the notch tip. The different specimens with several notch aspect ratios were tested with sandblasting on one face and two faces. Figure 6b shows one such specimen after testing.

The notch tip can be considered as a virtual crack after an effective distance X_{ef} [18]. The notch stress intensity factor K_{ρ} describes the stress distribution, defined as a function of the effective distance and effective stress in the case of the U-notch.

$$K_{\rho} = \sigma_{ef} \sqrt{2\pi X_{ef}} \tag{Eq 1}$$

Here, the effective stress σ_{ef} was considered as the average value of the stress distribution inside the fracture process zone. Justification of this approach and details were given in Refs. [19–23].

Results and Discussion

Mechanical Properties of API 5L X70 Pipe Line Steel

Effect of the Sample Orientation and Welded Zone

Typical tensile engineering stress–strain curves of the as-received API 5L X70 steel in different specimen directions

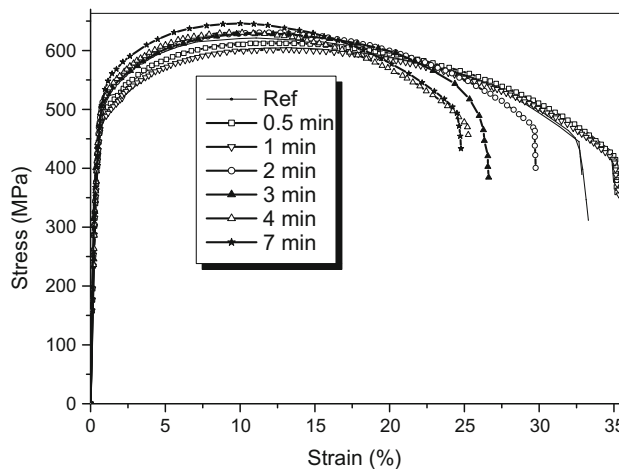


Fig. 8 Tensile test results for specimens prepared from the investigated API 5L X70 pipeline steel, in the rolling direction (R), with and without sandblasting for different times

Table 2 Average values of tensile properties of the base metal and the weld metal for API 5L X70 pipeline steel prepared from the R-, T- and L-directions

| API 5L X70 steel (average values) | | Young’s modulus E (GPa) | Yield stress (MPa) | Tensile strength (MPa) | Elongation (%) |
|-----------------------------------|------------|-------------------------|--------------------|------------------------|----------------|
| R-direction | Base metal | 217 | 491 | 631 | 38 |
| | Weld metal | 210 | 571 | 665 | 16 |
| L-direction | Base metal | 221 | 561 | 647 | 18 |
| T-direction | | 207 | 586 | 718 | 19 |

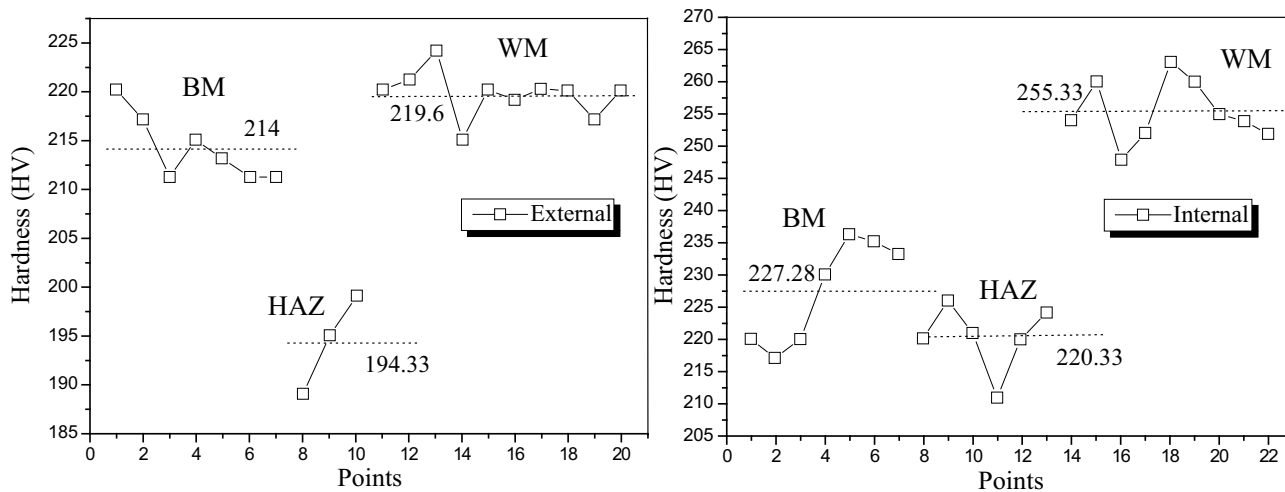
including weld metal are presented in Fig. 7. The behavior depicted by these curves is similar to that reported by Alhussein et al. [6] for API 5L X52 pipeline steel. The average values of tensile properties obtained from testing a minimum of three specimens taken from different positions of the same pipe are given in Table 2. All of the properties were found to meet the API 5L X70 specifications for line pipe steels [24].

The tensile properties of the API 5L X70 pipeline steel were obtained from specimens parallel to the rolling (R)-,

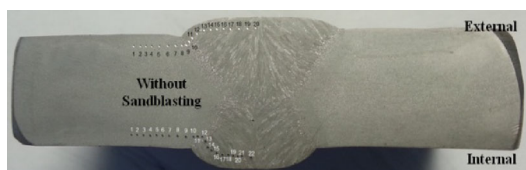
transverse (T)- and longitudinal (L)-directions in the base metal, as well as perpendicular to the rolling direction at the weld line. The average results of Table 2 show that because of anisotropy resulting from the thermomechanical processing of the pipe steel, all the mechanical properties are affected. Large variations exist between the properties in R-direction and T-direction, notably 19% difference in yield stress and 50% in elongation. These results are similar to those reported by Kim et al. [25]. As expected, the

Table 3 Tensile properties of the investigated API 5L X70 pipe steel with and without sandblasting at 90° impact angle

| API 5L X70 (average values) | Young’s modulus (GPa) | Yield stress (MPa) | Ultimate strength (MPa) | Elongation (%) | Thickness t (mm) |
|-----------------------------|-----------------------|--------------------|-------------------------|----------------|------------------|
| Reference | 212 | 506 | 612 | 34 | 13.10 |
| <i>t</i> = 0.5 min | 210 | 519 | 600 | 35 | 13.08 |
| <i>t</i> = 1.0 min | 207 | 530 | 612 | 35 | 13.03 |
| <i>t</i> = 2.0 min | 218 | 494 | 628 | 29 | 12.34 |
| <i>t</i> = 3.0 min | 214 | 496 | 628 | 26 | 12.12 |
| <i>t</i> = 4.0 min | 206 | 498 | 628 | 25 | 11.93 |
| <i>t</i> = 7.0 min | 204 | 515 | 645 | 24 | 11.44 |



(a)



Average values of the hardness on the external surface
 HV (BM) = 214
 HV (HAZ) = 194
 HV (WM) = 219

Average values of the hardness on the internal surface
 HV (BM) = 227
 HV (HAZ) = 220
 HV (WM) = 255

(b)

Fig. 9 Hardness results without sandblasting

weld material resulted in higher strength and lower ductility.

Sandblasting Effect on Tensile Properties

Figure 8 and Table 3 illustrate the effects of sandblasting duration on the tensile properties of API 5L X70 pipe steel for a nozzle angle of 90°. No significant adverse effect occurred at low impact times (≤ 1.0 min). The yield stress has increased by about 5% after 1.0 min of sandblasting. This is due mainly to surface plastic deformation and surface strengthening induced by the impact of sand grains. As will be seen in later section for these selected test conditions, there is no significant material removal and the weight loss up to 1.0 min is minimal. Most of the impact energy is converted into surface plastic deformation, and sandblasting may have had an effect similar to that of shot opening. Longer exposure to accelerated sand particles resulted in the reduction of yield strength and ultimate strength of the material. As observed by Hattori and Nakao [3], the period between 1.0 and 4.0 min may be considered as the acceleration stage in which an increasing number of superficial microcracks and craters are developed. Damage may have also been augmented by the interactions

occurring between different impacts. Finally, damage seems to stabilize after 4.0 min of sandblasting.

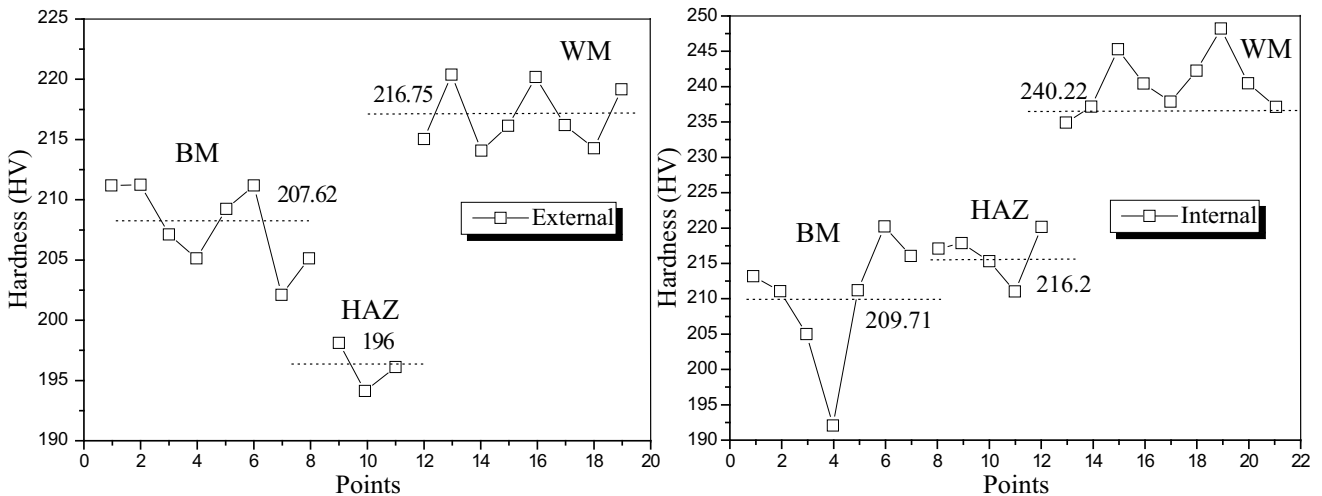
Effect of Sandblasting on Hardness

As shown in Figs. 9b and 10b, Vickers hardness measurements were taken in three zones BM, HAZ and WB at a distance of 2 mm from the internal and external edges of the pipe. Values of the measured hardness along with the average values in the three zones, without and with sandblasting, are presented in Figs. 9 and 10, respectively.

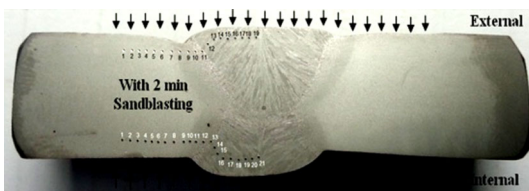
As expected, the results show that overall, the welding material has higher hardness than the HAZ and BM. Furthermore, there exists a difference in hardness between the internal and external surfaces, with the internal having 11–16% higher hardness. This may be due to the longer cooling rate of the internal weld passes being deposited first.

Time and Projection Angle Sandblasting on Charpy Specimens

The hardness tests result for the three zones (BM, WM and HAZ), different rolling directions and points across, the



(a)



(b)

Average values of the hardness on the external surface
 HV (BM) = 207
 HV (HAZ) = 196
 HV (WM) = 216

Average values of the hardness on the internal surface
 HV (BM) = 209
 HV (HAZ) = 216
 HV (WM) = 240

Fig. 10 Hardness result after 2.0 min of sandblasting on two faces

Table 4 Charpy energy values in each zone (BM, HAZ and WM) with and without sandblasting

| Zones | Average energy (Joules) without sandblasting | Average energy (Joules) with sandblasting (2 min) | Influence (%) | Ref. [26] without sandblasting |
|-------|----------------------------------------------|---------------------------------------------------|---------------|--------------------------------|
| BM | 206 | 40 | 80 | 214 |
| WM | 175 | 36 | 79 | 265 |
| HAZ | 242 | 56 | 76 | 202 |

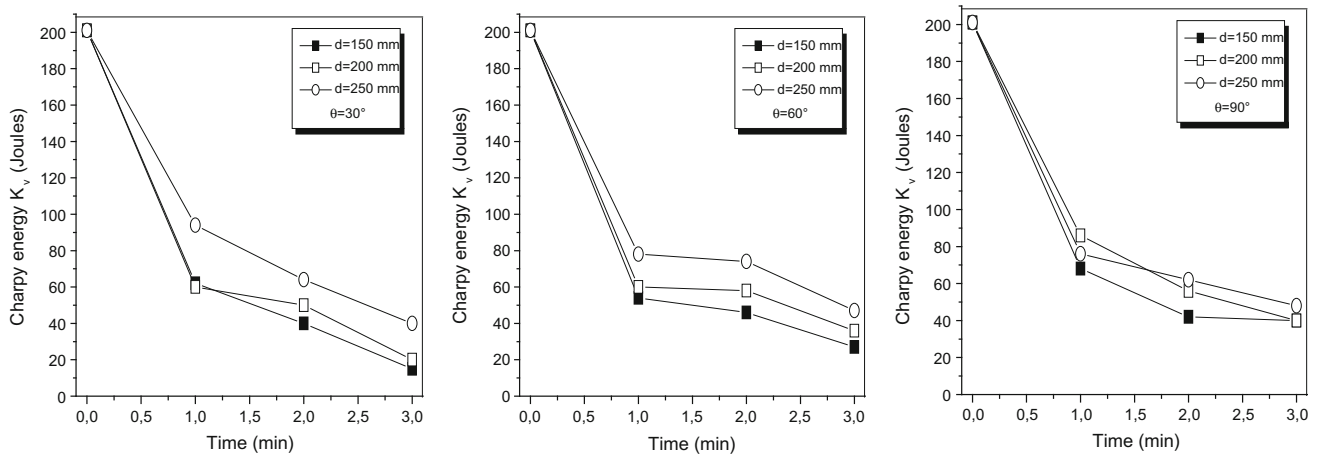


Fig. 11 Evaluation of the Charpy energy K_v as a function of the time of sandblasting for different angles of projection (90°, 60°, and 30°) and distances (150, 200, and 250 mm)

Table 5 Example of Charpy energy decreased by a percentage with the different angles of orientations

| Projection angle θ | Distance d (mm) | Time t (min) | Reference Charpy energy (Joule) | Charpy energy after sandblasting (Joule) | Differ. (%) |
|---------------------------|-------------------|----------------|---------------------------------|------------------------------------------|-------------|
| 90 | 150 | 3 | 206 | 40 | 80 |
| 60 | | | | 27 | 86 |
| 30 | | | | 15 | 92 |

wall thickness are presented in Table 4. The dimensions are fit in accordance with standard EN 10045-1 [16]. The sandblasting machine and the procedure to fix the specimens at different distances and angles are presented in “Sandblasting Setup” section. The Charpy V-notch impact test was conducted using a universal testing machine “BROOKS-type MAT21 IT3U” with a maximum capacity of 300 Joules. The test was carried out at ambient temperature, and the specimens were placed on the supports of the Charpy apparatus so that the edge of the knife struck it along the plane of symmetry of the notch and on the opposite surface. The hardness values of Charpy V-notch impact specimens are compared with results given in Ref. [25]. An example of the energy absorbed by the three zones, with and without sandblasting under 2 min, is presented in Table 4. The results for the base material show that the absorbed energies decrease with an increase in sandblasting time.

Secondly, the Charpy energy K_v of base metal was affected by three parameters: the blasting time from 0.5 to 3 min, the angles of impact projection of 30°, 60°, and 90°, and the blasting distance of 150, 200, and 250 mm. From the data obtained, the curves for the variation of the Charpy energy as a function of sandblasting time are plotted in Fig. 11.

The previous figure showed that the Charpy energy K_v decreases with blasting time and decreases with respect to blasting distance, impact angle. Table 5 shows that the Charpy energy decreases by 80% more, depending on decreasing the angles of impact.

Figure 12 shows an overall view of damage generated by the different positions of the sandblasting on steel surface. That the sizes of the defects are variable, and the defects are randomly scattered over the eroded surface. Observations of the exposed surfaces indicate the development of small craters, as well as the formation of lateral microcracks. Under repeated sand impacts, these

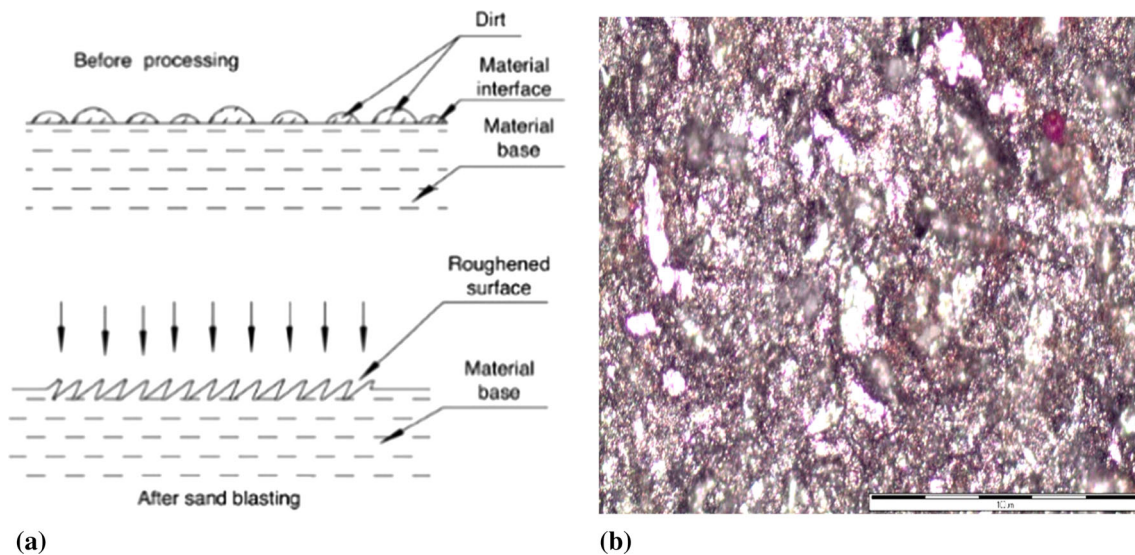


Fig. 12 Schematic damage surface near the notch tip after sandblasting Charpy V-notch impacting test (a) and microcracks in the surface (b)

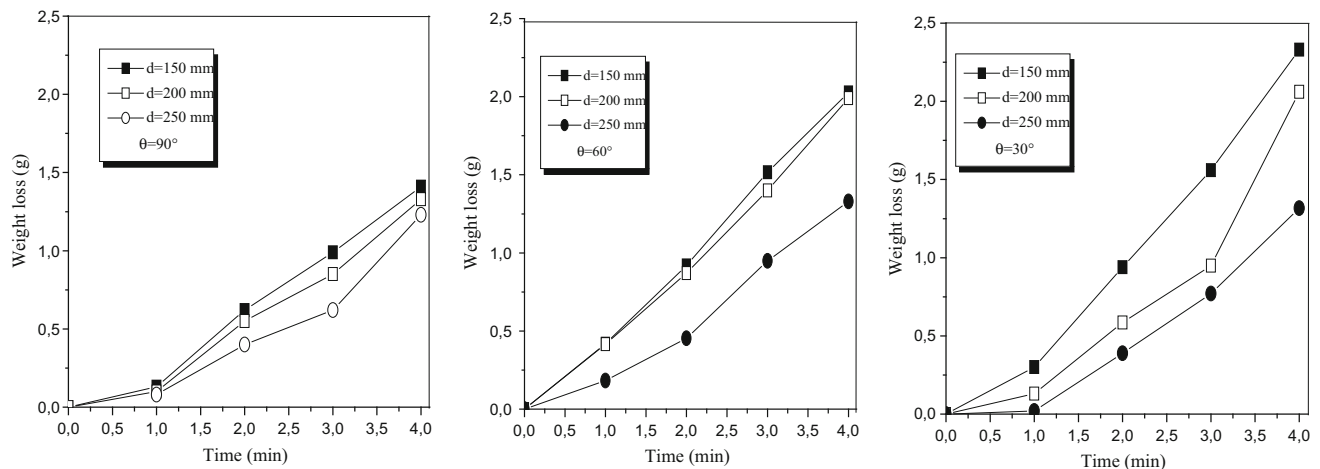


Fig. 13 Evolution of the weight loss on the longitudinal direction (L) as a function of the time of sandblasting for different angles of projection (90°, 60°, and 30°)

microcracks develop in the form of cracks. The impacted surface shown defects appear similar to the produced with the Vickers microhardness indentations. The theory of indentation shows that lateral microcracks are mostly caused by sharp particles or rounded particles but with relatively large impact forces. The damaged areas are different depending on the particle sizes. The density and damage of these defects increase with the projected masses of the particles impacting the surface.

Figures 13 and 14 show the influence of different parameters on the weight loss and the erosion rate of the Charpy V-notch specimens of the investigation API 5L X70 pipeline steel, respectively.

The weight loss during a sandblasting time at different projection angles is demonstrated in Fig. 13. The metal

loses its mass linearly with sandblasting time. This loss of mass increases with the decrease in the distance (Fig. 13a) and a decrease in the impact angle. At the critical angle of $\theta = 30^\circ$, at a maximum time of sandblasting and minimum distance, the metal loss reaches its maximum value among the test performed. Erosion rates of the steel specimens were measured from the slope of the weight loss versus time. Erosion rates were calculated by the following equation [26]:

$$E_0 = \left[\frac{\text{Weight loss, g}}{\left[\text{Specimen area, } \times \text{ density, g/mm}^3 \times \text{time, s} \right] \times 60 \text{ s/min} \times 60 \text{ min/h} \times 24 \text{ h/day} \times 365 \text{ day/year}} \right] \quad (\text{Eq 2})$$

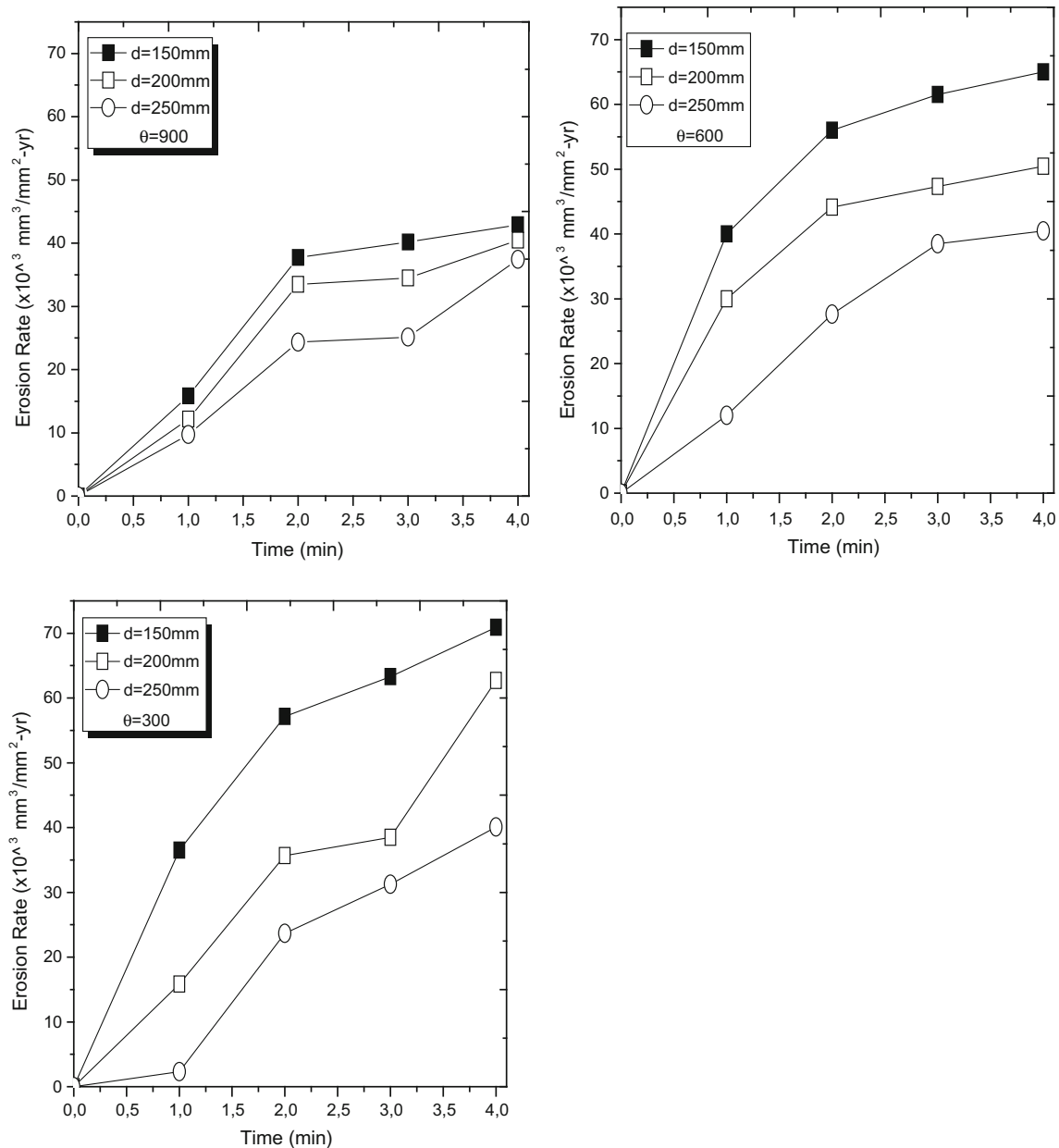


Fig. 14 Evolution of the erosion rate as a function of the time of sandblasting for different angles of projection (90° , 60° , and 30°) and distances (150, 200, and 250 mm)

The increase in erosion rate with an increase in sandblasting duration and/or with decrease in sandblasting distance is an expected. Furthermore, it can be seen that the erosion behavior with respect to impact angle is inverse relation, with a maximum erosion rate in the test at an angle 30° . Similar observations have been reported by other authors [27, 28]. Finnie et al. [29] observed that ductile materials generally show maximum erosion rates in the range of 15° – 30° impact angle, while brittle materials show maximum

erosion rate at normal angle. The erosion rate increases according to the sandblasting duration up to a constant value, Fig. 14. As expected, higher sandblasting duration leads to higher material removal from the surface as observed in other erosion studies of Hattori and Nakao [3].

Figure 15 shows the roughness profiles near the notch tip for a neat specimen without blasting and two attack times of 2 and 7 min in the orientation of 30° . It is observed that after 2 min of attack, the profile is still rather

Fig. 15 Profile of the roughness notch zone (a) before sandblasting (b) after 2 min and (c) after 7 min

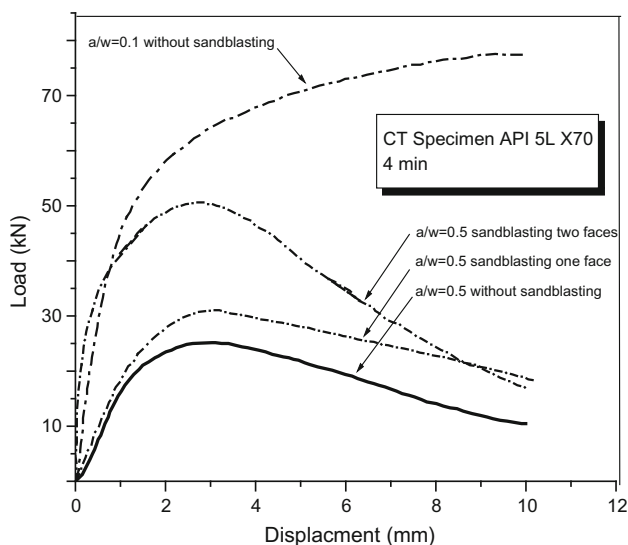
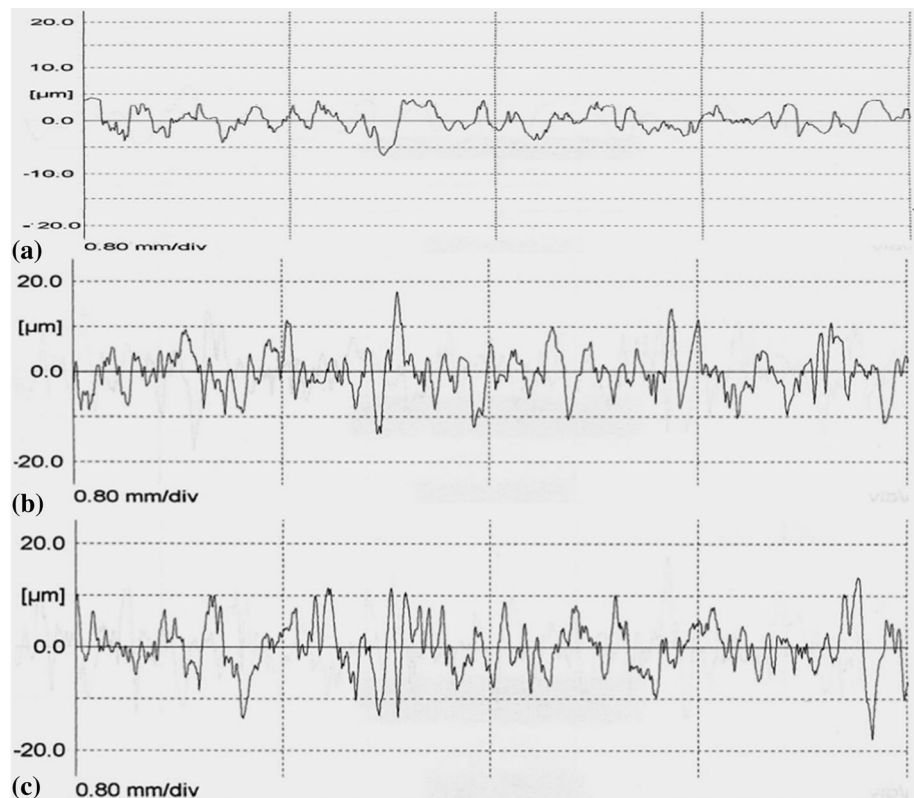


Fig. 16 Load vs. displacement on the investigated API 5L X70 pipeline steel for CT specimens with and without sandblasting ($a/W = 0.5$) compared to ($a/W = 0.1$) without sandblasting in the L-direction

sharp and that with time, it tends to attenuate to become rather rigorous for longer durations (7 min). The mean gap between troughs and ridges becomes larger.

Sandblasting Effect on Master Failure Material Curve (MFMC)

Effect of Sandblasting on the Load–Displacement Curve

The effects of sandblasting on fracture resistance with sandblasting on one or two faces and for both directions of pipeline [longitudinal (L) and transverse (T)] are presented as MFMC for API 5L X52 and API 5L X70 pipeline steels. The $K_p - T_{ef}$ curve is built with four specimen geometries (CT, SENT, RT and DCB) and a constant relative crack length $a/W = 0.5$. An example of the load–displacement graph is presented in Fig. 16 for a CT specimen after 4 min of sandblasting with relative crack length $a/W = 0.5$. Sandblasting was performed on one or two faces for the CT, SENT and DCB specimens, while the RT specimens were sandblasted on one face. For comparison, the same specimen type without sandblasting with two relative crack lengths ($a/W = 0.1$ and $a/W = 0.5$) is also presented.

The value of the maximum load after 4 min of sandblasting on one (RT) and two faces (CT, SENT and DCB) for the four specimen geometries is summarized in Table 6.

Table 6 Recapitulation of the maximum loading on the load–displacement graph for X70 steel in the L-direction

| Specimens | | Without sandblasting | Type of sandblasting | | Max. load (kN) | Av. value max load (kN) |
|-----------|-------|----------------------|----------------------|-----------|----------------|-------------------------|
| | | | One face | Two faces | | |
| DCB | DCB1 | ✓ | | | 23.67 | 25.75 |
| | DCB2 | ✓ | | | 27.83 | |
| | DCB3 | | ✓ | | 28.61 | 32.93 |
| | DCB4 | | ✓ | | 35.87 | |
| | DCB5 | | ✓ | | 34.31 | 51.85 |
| | DCB6 | | | ✓ | 56.24 | |
| | DCB7 | | | ✓ | 45.48 | |
| | DCB8 | | | ✓ | 53.83 | |
| RT | RT1 | ✓ | | | 35.55 | 34.33 |
| | RT2 | ✓ | | | 33.11 | |
| | RT3 | | ✓ | | 31.11 | 35.69 |
| | RT4 | | ✓ | | 36.92 | |
| | RT5 | | ✓ | | 39.06 | 56.25 |
| | RT6 | | | ✓ | 61.56 | |
| | RT7 | | | ✓ | 50.03 | |
| | RT8 | | | ✓ | 57.16 | |
| CT | CT1 | ✓ | | | 33.21 | 31.26 |
| | CT2 | ✓ | | | 29.31 | |
| | CT3 | | ✓ | | 34.08 | 38.09 |
| | CT4 | | ✓ | | 39.01 | |
| | CT5 | | ✓ | | 41.19 | 59.51 |
| | CT6 | | | ✓ | 62.58 | |
| | CT7 | | | ✓ | 55.53 | |
| | CT8 | | | ✓ | 60.44 | |
| SENT | SENT1 | ✓ | | | 29.01 | 29.58 |
| | SENT2 | ✓ | | | 30.15 | |
| | SENT3 | | ✓ | | 36.36 | 41.61 |
| | SENT4 | | ✓ | | 42.89 | |
| | SENT5 | | ✓ | | 45.57 | 63.69 |
| | SENT6 | | | ✓ | 65.98 | |
| | SENT7 | | | ✓ | 60.23 | |
| | SENT8 | | | ✓ | 64.88 | |

Table 7 Linear relationship parameters A and B comparison in the MFMC

| Parameter | X70 without sandblasting | X52 without sandblasting | X70 with sandblasting, one face | X70 with sandblasting, two faces | X52 with sandblasting, one face |
|-----------|--------------------------|--------------------------|---------------------------------|----------------------------------|---------------------------------|
| A | −0.0484 | −0.074 | −0.049 | −0.048 | −0.068 |
| B | 93.30 | 77.96 | 114.05 | 113.57 | 83.94 |

Effect of Sandblasting on MFMC

The different MFMCs obtained for different conditions of sandblasting and for the two steels (API 5L X52 and API 5L X70) are fit with a linear relationship:

$$K_{\rho,c} = AT_{ef,c} + K_{\rho,c}^0 \tag{Eq 3}$$

where *A* is a material constant and $K_{\rho,c}^0$ is the reference notch fracture toughness for $T_{ef,c} = K_{\rho,c}^0$. Value of *A* and $K_{\rho,c}^0$ is reported in Table 7.

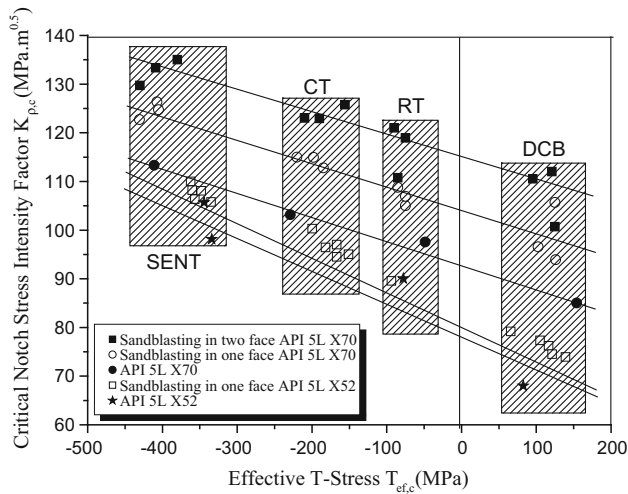


Fig. 17 Different MFMCs according to sandblasting conditions for two pipe steels API 5L X70 and API 5L X52 steel

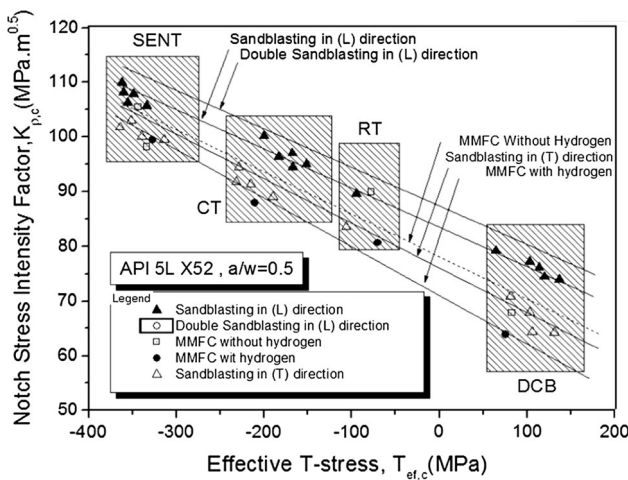


Fig. 18 MFMC for the different API 5L X52 pipeline specimens for $a/w = 0.5$ [30, 32]

The slopes A of the different MFMCs are similar. The reference notch fracture toughness, $K_{\rho,c}^0$, increases for sandblasting and for the two steels indicating a beneficial effect.

Figure 17 presents amelioration of notch fracture toughness with sandblasting curves. The upward shift of the reference notch fracture toughness, $K_{\rho,c}^0$, is about 15% for one face and 28% for two faces. The beneficial effect of sandblasting is due to three main parameters (1) the local hardening created near the notch tip, (2) the residual stresses are in compression under the notch, and (3) the increase in the notch radius during the sandblasting tests.

The effect of the microstructure in (L)- and (T)-directions is noticeable in the difference on the MFMC of the two situations. This deviation is ascribed to exploit specimens between the tensile and flexion loading. The decrease in the notch stress intensity factor values for different specimens is related to the degree of constraint around the crack. Increasing the yield stress increases the constraint parameter. Figure 18 is presented in order to examine the effect of the second terms of Williams [31] solutions, i.e., effective stress intensity factor for the different shape of specimen's with the presence of two directions (L) and (T), the double sandblasting or faces and the hydrogen charging [32].

The fracture toughness variation of the pipeline API 5L X70 steel eroded by sandblasting is more appropriate to the material damage at and near the notch tip. An optical and scanning electron microscope (SEM) was taken from the Figs. 19 and 20 respectively. These images illustrate the crack tips in material after failure. Classical cracks create and propagate in the direction perpendicular to the principal stress. The observed cracks appeared to be formed by cleavage, and the propagation seems to be intragranular, see Fig. 19a. After sand erosion, cracks initiate in

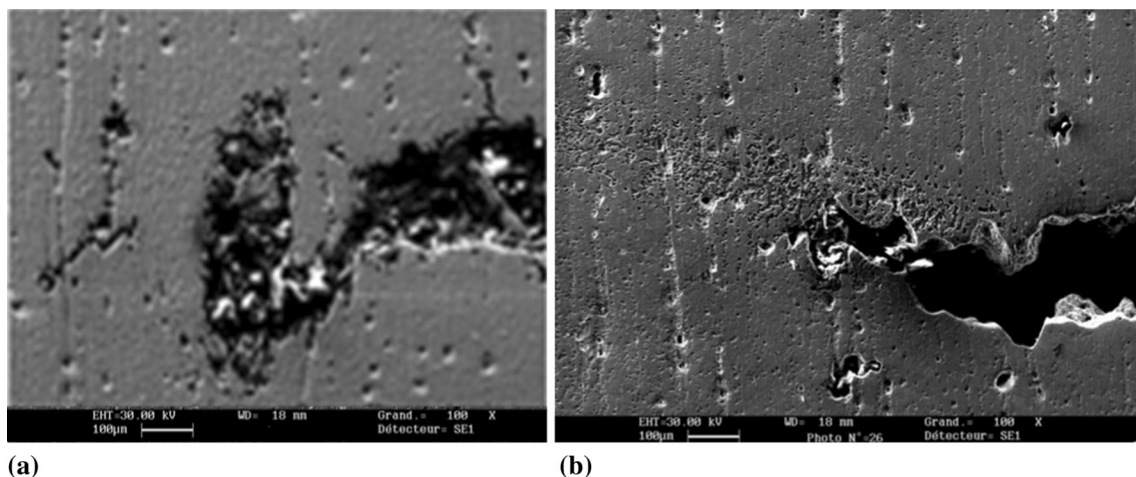


Fig. 19 Scanning electron photomicrographs of polished cross sections through cracked for CT specimen: (a) compared to the failure section in air, (b) zoom magnification

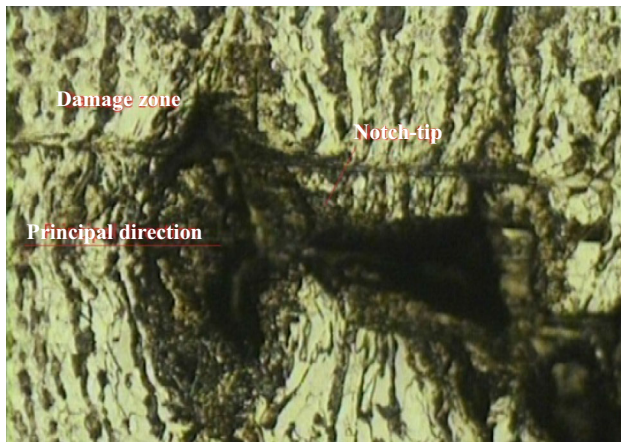


Fig. 20 Observation of crack propagation in material by optical microscopy (after etching with Nital)

privileged sites outside of cracking plane. The deformation field is very important with a very large deformation on the material flow. Figure 20 illustrates the crack propagation in material using optical microscopy after chemical etching with Nital. The damage zone by sandblasting stopped the crack propagation in the principal direction and the smooth notch tip will be created. More concentrations zones will be created near the notch tip, increasing on the fracture toughness of the sandblasting material.

Conclusion

The effect of sandblasting on mechanical properties and Material Failure Master Curves (MFMC) of API 5L X52 and API 5L X70 pipeline steels was analyzed from a viewpoint of notch fracture mechanics. The investigation of the effect of sandblasting duration on the erosion behavior and mechanical property of API 5L X70 pipeline steel showed that the sandblasting has two principal effects. The results demonstrated that the sandblasting has slightly increased the yield stress, the ultimate strength and the fracture toughness and, at the same time, had an adverse effect on elongation, young's modulus, hardness and thickness of the tested pipeline. Despite the erosion of these layers, under the sand impacting, failure strain and rate of degradation are improved. The observation of failure mode shows that the deformation field, after sandblasting, is very important.

The MFMC based on the two-parameter fracture criterion has been determined for API 5L X70 pipeline steels. The notch fracture toughness $K_{\rho,c}$ and the effective T-stress were employed to describe the Material Failure Master Curve. A strain gauge technique was applied on notched specimen tests under static loading. The notch fracture

toughness is a linear function of the $T_{ef,c}$ -stress. The influence of sandblasting in the different directions (L) and (T) and the two faces, on a surface notched pipeline with API 5L X70 steel, was studied based on the laboratory SENT, CT, RT (Roman Tile) and DCB specimens. An experimental comparison of Master Failure Material Curves for sandblasting on the API 5L X52 was made to determine the degrees of degradation. The mechanical properties for material with and without sandblasting can be applied as an engineering parameter for structural integrity assessment of pipelines.

References

1. R.J.K. Wood, T.F. Jones, Investigations of sand-water induced erosive wear of AISI 304L stainless steel pipes by pilot-scale and laboratory-scale testing. *Wear* **255**, 206–218 (2003)
2. X. Hu, A. Neville, CO₂ erosion–corrosion of pipeline steel (API X65) in oil and gas conditions a systematic approach. *Wear* **267**(11), 2027–2032 (2009)
3. S. Hattori, E. Nakao, Cavitation erosion mechanisms and quantitative evaluation based on erosion particles. *Wear* **249**, 839–845 (2002)
4. Suyitno, B. Arifvianto, T.D. Widodo, M. Mahardika, P. Dewo, U.A. Salim, Effect of cold working and sandblasting on the microhardness, tensile strength and corrosion resistance of AISI 316L stainless steel. *Int. J. Miner. Metall. Mater.* **19**(12), 1093 (2012)
5. A. Alhussain, J. Capelle, J. Gilgert, S. Dominiak, Z. Azari, Influence of sandblasting and hydrogen on tensile and fatigue properties of pipeline API 5L X52 steel'. *Int. J. Hydrog. energy* **36**, 2291–2301 (2011)
6. A. Alhussain, J. Capelle, J. Gilgert, A. Tidu, S. Hariri, Z. Azari, Static, dynamic and fatigue characteristics of the pipeline API 5L X52 steel after sandblasting'. *Eng. Fail. Anal.* **27**, 1–15 (2013)
7. P.C. Okonkwo, R.A. Shakoor, E. Ahmed, A.M.A. Mohamed, Erosive wear performance of API X42 pipeline steel. *Eng. Fail. Anal.* **60**, 86–95 (2016)
8. D. Lopez, J.P. Congote, J.R. Cano, A.P. Toro, A.P. Tschiptschin, Effect of particle velocity and impact angle on the corrosion–erosion of AISI 304 and AISI 420 stainless steels. *Wear* **259**, 118–124 (2005)
9. M. Aminul Islam, Z.N. Farhat, E.M. Ahmed, A. Alfantazi, Erosion enhanced corrosion and corrosion enhanced erosion of API X70 pipeline steel. *Wear* **302**, 1592 (2013)
10. Z.A. Majid, R. Mohsin, Multiple failures of API 5L X42 natural gas pipeline. *Eng. Fail. Anal.* **31**, 421–429 (2013)
11. I. Finnie, G.R. Stevick, J.R. Ridgely, The influence of impingement angle on the erosion of ductile metals by angular abrasive particles. *Wear* **152**(1), 91–98 (1992)
12. R.K. Chintapalli, A. Mestra, F.G. Marro, M. Anglada, Effect of sandblasting and residual stress on strength of zirconia for restorative dentistry applications. *J. Mech. Behav. Biomed. Mater.* **29**, 126–137 (2014)
13. <http://www.sonatrach.com/en/transport-par-canalisation.html/2012>
14. ISO 15614, *Specification and Qualification of Welding Procedures for Metallic Materials—Welding Procedure Test—Part 5: Arc Welding of Titanium, Zirconium and Their Alloys* (2004)
15. ASTM, *G119-09, Standard Guide for Determining Synergism Between Wear and Corrosion, Annual Book of ASTM Standards, Vol 03.02* (ASTM International, West Conshohocken, 2009)

16. NF EN 10045-1, *Essai de flexion par choc sur éprouvette Charpy, partie 1: Méthode d'essai*, Association Française de Normalisation (AFNOR, 1990)
17. ASTM E92-82(2003)e2, *Standard Test Method for Vickers Hardness of Metallic Materials (Withdrawn 2010)* (ASTM International, West Conshohocken 2003), www.astm.org
18. J. Capelle, Etude de la nocivité d'un défaut de type éraflure sur une conduite destinée au transport de gaz naturel soumise à une pression d'hydrogène, Thèse de doctorat, Laboratoire de Fiabilité Mécanique, LFM, Ecole d'Ingénieur de Metz-ENIM-, France, 2008
19. M. Hadj Meliani, G. Pluvinage, Y.G. Matvienko, Two parameter fracture criterion (K_p -Tef) derived from notch fracture mechanics. *Int. J. Fract.* **167**, 173–182 (2011)
20. G. Pluvinage, *Fracture and fatigue emanating from stress concentrators* (Springer, Netherlands, 2003)
21. M. Hadj Meliani, Y.G. Matvienko, G. Pluvinage, Corrosion defect assessment on pipes using limit analysis and notch fracture mechanics. *Eng. Fail. Anal.* **18**, 271–283 (2011)
22. T. Nateche, M. Hadj Meliani, S.M.A. Khan, Y.G. Matvienko, N. Merah, G. Pluvinage, Residual harmfulness of a defect after repairing by a composite patch. *Eng. Fail. Anal.* **48**, 166–173 (2015)
23. A. El-Azzizi, M. Hadj Meliani, A. Khelil, G. Pluvinage, Y.G. Matvienko, The master failure curve of pipe steels and crack paths in connection with hydrogen embrittlement. *Int. J. Hydrog. Energy* **40**, 2295–2302 (2015)
24. O. Bouledroua, M.O. Mbereick, M. Hadj Meliani, Qualification d'un acier API 5L X70: étude expérimentale et validation numérique. *Nat. Technol. A Sci. Fondam. Eng.* **13**, 34–39 (2015)
25. Y.M. Kim et al., Effects of molybdenum and vanadium addition on tensile and charpy impact properties of API X70 linepipe steels. *Metall. Mater. Trans. A* **38**(8), 1731–1742 (2007)
26. T. Bellahcene, Etude de la nocivité des défauts dans les canalisations sous environnement hydrogène, Doctoral Thesis, Mouloud Mammeri University of Tizi-Ouzou, Algeria, 2012.
27. Y.I. Oka, H. Ohnogi, T. Hosokawa, M. Matsumura, The impact angle dependence of erosion damage caused by solid particle impact. *Wear* **203–204**, 573 (1997)
28. C.T. Morrison, R.O. Scattergood, J.L. Routbort, Erosion of 304 stainless steel. *Wear* **111**, 1 (1986)
29. G.L. Sheldon, I. Finnie, On the ductile behavior of nominally brittle materials during erosive cutting. *J. Eng. Ind.* **88**, 387 (1965)
30. I. Finnie, G.R. Stevick, J.R. Ridgely, The influence of impingement angle on the erosion of ductile metals by angular abrasive particles. *Wear* **152**, 91–98 (1992)
31. M.L. Williams, *J. Appl. Mech.* **24**, 109–114 (1957)
32. M. Hadj Meliani, O. Bouledroua, A. Alhussein, Y.G. Matvienko, G. Pluvinage, Some aspects of sandblasting and hydrogen on the material master failure Curve in engineering fracture mechanics. *Anales de Mecánica de la Fractura* **32**, 94–103 (2015)